Tectonophysics 683 (2016) 172–181

Contents lists available at ScienceDirect

Tectonophysics

journal homepage: www.elsevier.com/locate/tecto

Geomechanical analysis of a welding salt layer and its effects on adjacent sediments

Mahdi Heidari [a,*], Maria A. Nikolinakou [a], Michael R. Hudec [a], Peter B. Flemings [b]

[a] Bureau of Economic Geology, The University of Texas at Austin, 10100 Burnet Road, Building PRC-130, Austin, TX 78758, USA

[b] Department of Geological Sciences and Institute for Geophysics, Jackson School of Geosciences, The University of Texas at Austin, 10100 Burnet Road, Building PRC-130, Austin, TX 78758, USA

ARTICLE INFO

Article history:
Received 4 January 2016
Received in revised form 10 June 2016
Accepted 20 June 2016
Available online 23 June 2016

Keywords:
Salt weld
Stress near salt
Salt-weld seal
Salt diapirism modeling
Wellbore stability

ABSTRACT

We simulate welding of the source layer of a salt diapir with a forward finite-element model and study stresses and deformation in the salt layer and the diapir, as well as in their adjacent sediments. Welded salt layers are abundant in mature salt basins, where most or all of the salt has withdrawn into diapirs. However, there is little understanding of the stress field in these layers and their adjacent sediments. We show that salt flow along the source layer leads to significant stress anomalies inside the layer and in adjacent sediments. In the source layer, salt pressure becomes higher than overburden stress in nearly welded areas and becomes lower than overburden stress in adjacent thicker areas. When the source layer welds, stresses increase significantly in sediments near the weld tip, which helps compaction of these sediments and possibly their fracturing and faulting. Our model illustrates that all sediments overlying the weld experience this stress increase and the associated material changes as the weld tip propagates along the weld. We present natural examples fitting our predictions and discuss the importance of our results for the exploration, characterization, and production of reservoirs near welded salt layers.

1. Introduction

Horizontal salt welds, also known as primary welds, develop by complete or almost complete withdrawal of salt from a source layer into diapirs (Jackson and Talbot, 1991) (Fig. 1a). Several studies have documented geologic attributes of these welds and their importance to hydrocarbon exploration (Hoetz et al., 2011; Jackson et al., 2014; Maione, 2001; Peel, 2014; Rowan et al., 2012; Wagner, 2010). For instance, Hoetz et al. (2011) studied the data from wells drilled through horizontal welds and found a consistent reduction in the porosity of sediments near the welds. Maione (2001) also reported steeply dipping faults in sediments above salt welds in the East Texas Basin. However, there is little understanding of the linkage between these attributes and the welding process. Because the stress field near the welds determines these structural attributes, understanding the linkage requires identifying the stress field near a welding salt layer and the controls that the welding process has on the field.

To our knowledge, only one study has considered stresses near salt welds (Hoetz et al., 2011). The authors simulated a source-layer weld with a simplified model representing the overburden as a rigid sediment block sitting on a horst in a sea of salt (the "brick in a bathtub" model in their terminology). With analytical and numerical calculations, they showed that vertical stress increases remarkably at the base of the sediment block where the block is supported by the horst. However, in their simplified analysis, the authors studied only the vertical stress; further, because they assumed no limit for sediment strength (i.e., purely elastic behavior), they overestimated the stress increase at the weld. In addition, they simulated only the present geometry of the weld. As a result, their study fails to provide the history of stresses and possible irreversible material changes in sediments that could have occurred in the past during weld development.

Drilling results, along with analytical and numerical models, have shown that horizontal stress is high near vertical flanks of diapirs with a thick source layer in extensional or passive-margin basins (Dusseault et al., 2004; Heidari et al., 2016; Nikolinakou et al., 2014) (Fig. 1b). However, it is not clear whether this horizontal stress remains high after the source layer of the diapirs thins and welds. The high horizontal stress in diapir-flank sediments results from high horizontal pressure from the diapir pushing laterally against the sediments (Dusseault et al., 2004). Heidari et al. (2016) showed that the source layer of a salt diapir contributes to the high salt pressure in the diapir. They showed that the salt in the source layer is overpressured relative to the salt in the diapir and that the salt flow from the source layer into the diapir transmits this overpressure to the latter, increasing its own salt pressure. The magnitude of the transmitted overpressure

* Corresponding author.
E-mail addresses: mahdiheidari@utexas.edu (M. Heidari), mariakat@mail.utexas.edu (M.A. Nikolinakou), michael.hudec@beg.utexas.edu (M.R. Hudec), pflemings@jsg.utexas.edu (P.B. Flemings).

http://dx.doi.org/10.1016/j.tecto.2016.06.027

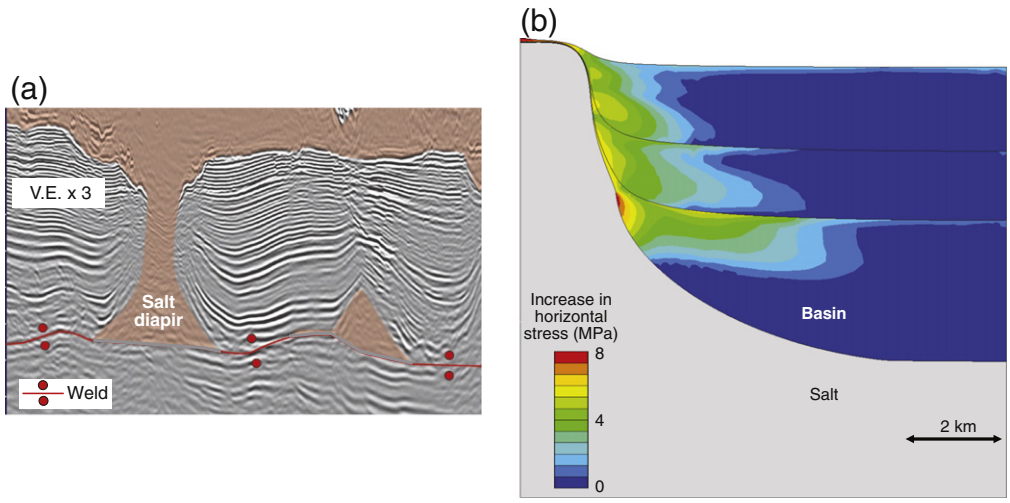

Fig. 1. Diapirs with welded and thick source layers. (a) A salt diapir with a largely welded source layer in Gulf of Mexico. Seismic data courtesy of CGG. (b) Increase in horizontal stress near a salt diapir with a thick source layer relative to regional (far-salt) value, obtained from a numerical model (Nikolinakou et al., 2014). High horizontal stress in diapir-flank sediments results from salt pressure, which is equal to salt overburden stress plus additional overpressure from salt source layer.

depends on the salt-pressure dissipation along the source layer, which changes with the source-layer thickness and geometry (Langlois and Deville, 2014). To quantify this dissipation and therefore the salt pressure in the diapir as the source layer thins and welds, one needs to simulate the salt flow along with the evolution of the source-layer geometry.

Many hydrocarbon prospects lie near salt diapirs with a welded source layer. Changes in stresses and structural attributes of sediments near welds are important for the exploration and production of these prospects. Stresses have direct control of the stability of wellbores and therefore of the planning of safe and economic drilling operations (Dusseault et al., 2004; Luo et al., 2012). The porosity of sediments affects the productivity of reservoirs, and the existence of faults impacts the migration and trapping of hydrocarbons. The geomechanical analysis of welding can thus also help better exploration, characterization, and production of reservoirs near welded salt layers.

In this study, we use a forward evolutionary finite-element model to investigate the impact of source-layer welding on stresses in the salt layer and diapir, as well as in their adjacent sediments. Our model, using realistic geometries of a salt-basin system, allows us to study stresses for a spectrum of source-layer thicknesses ranging from thick to thin to, finally, welded. We use more realistic poroelastic–plastic rheology for sediments (Albertz and Sanz, 2012; Gray et al., 2014), thereby taking into account their finite strength. Our model also allows us to monitor stresses through the entire process of welding and thereby identify possible irreversible stress-related features in sediments.

2. Numerical model

We use a plane-strain finite-element model to simulate the rise of a salt wall and the subsequent welding of its source layer under progressive sedimentation. The model is built within Elfen® (Rockfield, 2010) and analyzed using a finite-deformation, quasistatic, explicit, Lagrangian formulation with automated adaptive remeshing to handle excessive distortion of elements during large deformations (Peric and Crook, 2004; Thornton et al., 2011). A new mesh of elements is generated once a set of predefined criteria for element distortion is exceeded in any region in the model (Perić et al., 1999). The program also uses a regularization method to eliminate the dependency of results on the element size distribution in strain-softening regions.

Salt is represented as a viscoplastic material (Munson, 1997) with a constant density of 2.1 g/cm^3 (Fig. 2) and a viscosity that decreases with depth because of ground-temperature gradient. Sediments are represented by a critical-state poroelastic–plastic material model, SR3 (Crook et al., 2006). SR3 maintains the advantages of a traditional Mohr–Coulomb model to define sediment failure under shear stress and also takes into account material inelastic behavior under isotropic stresses (Muir Wood, 1990). Our model considers compaction of sediments with depth and the resulting increase in their density (Fig. 2). The input parameters used for salt and sediments in our model are given in Appendix A. The sediment parameters in our model reflect the behavior of a mudrock (Rockfield, 2010). Mudrocks are very common in most passive margin systems, which are of particular interest in salt tectonics (Boggs, 2010). For the sake of simplicity, only one rock type is used in the model.

Our model initiates with a flat salt layer having 3 km thickness and 60 km breadth (Fig. 3a). Sediments are deposited with a slope of 2° toward the center of the model and the final sediment thickness of 18 km. Sedimentation is simulated by progressive deposition of sediment

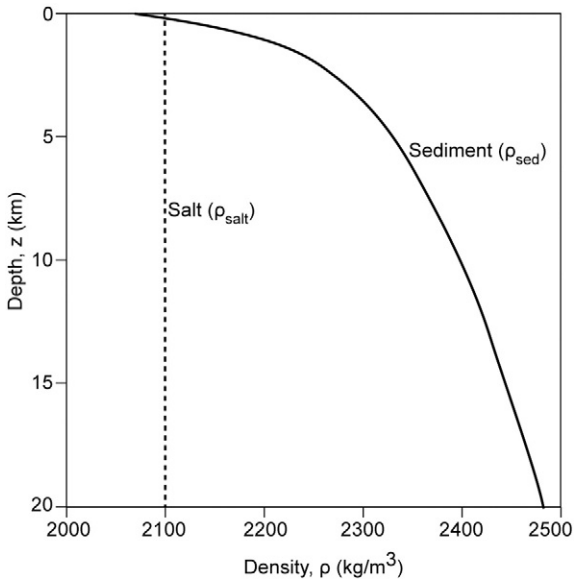

Fig. 2. Density profiles of salt and sediments. With depth, salt has a constant density, but sediments increase in density because of compaction.

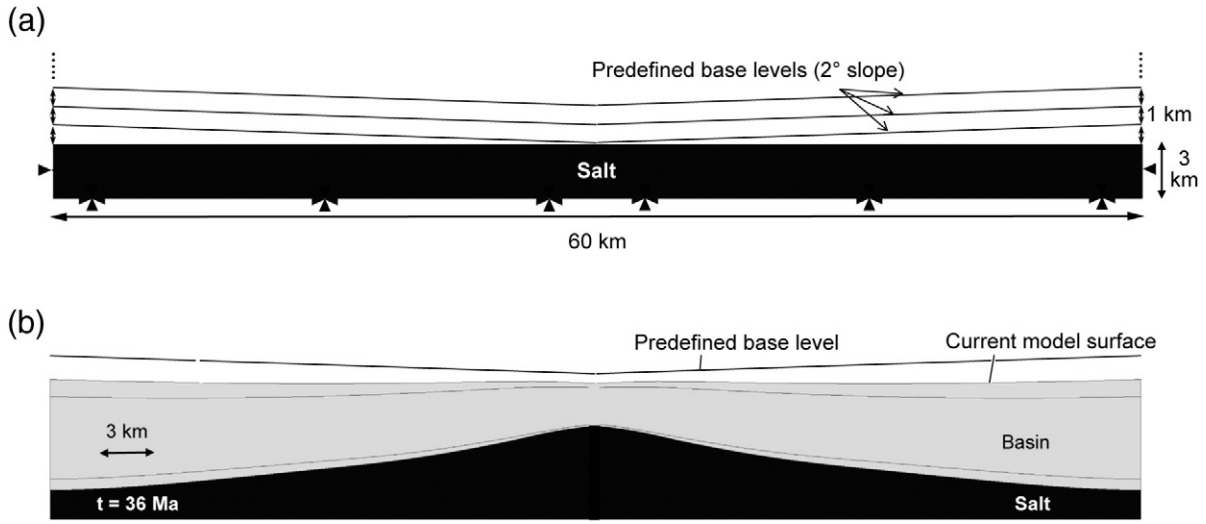

Fig. 3. Initial geometry of model and sedimentation process. (a) Initial geometry and predefined base levels of sedimentation. A flat salt layer with an initial thickness of 3 km and breadth of 60 km are overlain by sediments deposited according to a series of predefined parallel base levels with an interval of 1 km and converging with a 2° dip toward center of model. (b) Process of base-level rise. At each base-level rise event in model, sediments are deposited between base level defined for that event and current model surface.

layers. Each sediment layer fills the gap between the predefined base-level for that layer and the present surface of the model (Fig. 3b). Thus, the thickness of each layer depends on the topography immediately prior to its deposition. This configuration simulates bidirectional progradation converging toward the center of the salt layer. Progradation is a common way to initiate salt diapirism (Hudec and Jackson, 2011).

Sediments are deposited with an initial porosity of 38% (Thornton and Crook, 2014), which decreases as the sediments are buried and compressed by subsequent deposits, leading to an increase in density with depth. Each 1-km sediment layer is deposited every 10 Ma, representing a base-level rise rate of 0.1 km/Ma, which is at the low end of the natural range of base-level rise rates (Huffman et al., 2002). The weight of the sediment layer is applied gradually over this period.

Displacement of sediments and salt at the model side boundaries are allowed vertically and constrained laterally. Displacement of salt and basin sediments along the weld are constrained both laterally and vertically at the basal boundary. No slip is allowed at the salt-sediment interface. Pore pressure in basin sediments is assumed hydrostatic throughout the analysis; that is, the model is drained.

Differential loading of the salt layer by basin sediments causes expulsion of salt from the source layer into the rising salt diapir (Fig. 4a–f). Expulsion of salt continues until the source layer thins and then welds at an intermediate point along the salt base (Fig. 4f). In our model, welding—full evacuation of salt from a nearly welded area of the source layer—is implemented by replacing salt in the source layer with sediments where source-layer thickness becomes lower than 50 m (time = 80–85 Ma; Fig. 4f, g). The weld then propagates toward the salt diapir, reducing the width of the diapir pedestal—the part of the source layer between the weld tip and the diapir (Fig. 4g, h).

3. Salt pressure

3.1. General principles

Salt withdrawal from a source layer into its adjacent diapir causes the salt pressure in the diapir to become higher than the salt overburden stress. In a simple diapir model (Fig. 5a) (Heidari et al., 2016), the weight of the basin causes pressure in the source layer equal to ($\sigma_{ob,\ basin}$, Fig. 5a)

$$\sigma_{ob,\ basin} = \int_{basin} \rho_{sed}(z) g dz \tag{1}$$

The salt isostatic pressure in the source layer, resulting from the weight of the salt diapir and its roof, $\sigma_{ob,\ \ diapir}$, equals (Fig. 5a)

$$\sigma_{ob,\ diapir} = \int_{diapir} \rho_{salt}\, g\, dz + \int_{roof} \rho_{sed}\, g\, dz \tag{2}$$

Salt withdrawal from the source layer into the diapir occurs when $\sigma_{ob,\ \ basin} > \sigma_{ob,\ \ diapir}$. If $\sigma_{ob,\ \ basin} = \sigma_{ob,\ \ diapir}$, the salt is in static equilibrium and does not withdraw. Thus, in withdrawing source layers, the salt pressure is higher than isostatic pressure by an overpressure equal to

$$\Delta P = \sigma_{ob,\ basin} - \sigma_{ob,\ diapir} \tag{3}$$

Salt overpressure ΔP dissipates with the salt flow along the source layer and then up the diapir. When the source layer is thick relative to the diapir's width, the majority of the dissipation takes place along the diapir and dissipation along the source layer is minimal. In this case, the salt overpressure equals ΔP at the base of the diapir and dissipates linearly up the diapir (Fig. 5) (Heidari et al., 2015), resulting in pressure in the diapir that is higher than its salt overburden (isostatic) stress (Fig. 5b).

The magnitude of overpressure ΔP depends on the density profile of salt and basin sediments, and on the thickness of the diapir and basin. We calculate ΔP for the density profiles used in this study (Fig. 2) and salt diapirs at the basin surface (diapir height = basin thickness; Fig. 5a). The magnitude of ΔP relative to the diapir overburden stress, $\sigma_{ob,\ \ diapir}$, increases with basin thickness, reaching nearly 10% for a basin thickness of 10 km (Fig. 6).

3.2. Model results

We use our numerical evolutionary model to evaluate salt overpressure as the source layer thins and welds. We then compare the resulting total salt pressure to the overburden stress along the source layer to evaluate their possible difference during source-layer thinning and welding.

3.2.1. Salt overpressure

We calculate salt overpressure normalized by diapir overburden stress along a horizontal line passing through the middle of the source layer at different times during source-layer thinning and welding (Fig. 7a). To obtain the salt overpressure at each time, we calculate diapir overburden stress (isostatic pressure) from the height of the diapir

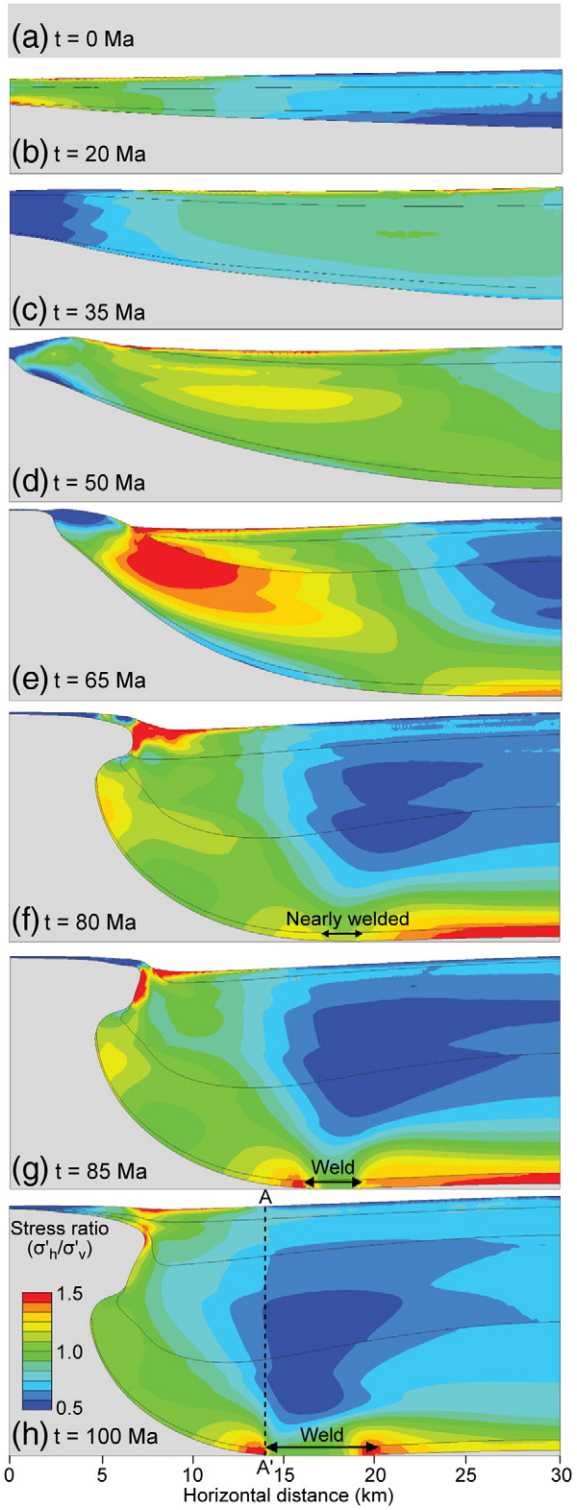

Fig. 4. Evolution of salt-basin system during progressive sedimentation. Given symmetry of model, only right half of model is shown. Contours in basin show horizontal to vertical stress ratio at each stage. Low ratios (blue) indicate lateral extension, and high ratios (red) indicate lateral compression of sediments. (a) Initial flat salt layer. (b) Upbuilding of salt diapir as a result of differential loading. (c) Diapir rising, which causes lateral extension of roof sediments. (d) Extrusion of salt diapir to basin surface. Lateral extension of roof sediments causes their extensional failure and intensive thinning. (e) Lateral expansion of salt diapir concurrent with salt withdrawal and thinning of source layer. (f) Just before source-layer welding begins. (g) Shortly after source-layer welding begins. (h) Final configuration of salt diapir and source-layer weld. Horizontal stress increases significantly down vertical profile A-A′ and decreases at upper levels.

and its roof using salt and sediment-density profiles ($\sigma_{ob,\ diapir}$, Eq. (2); Fig. 2) and subtract the stress from the salt pressure given by the model. Because diapir overburden stress changes over time, we do not compare normalized salt overpressures at different times.

Salt overpressure along the source layer and at the diapir base changes significantly as the geometry of the source layer changes during the thinning and welding of the layer. In early stages, thickness of the source layer is almost uniform (Fig. 4b); accordingly, salt overpressure dissipates along the source layer with an almost uniform gradient (time = 20 Ma; Fig. 7a). Because the diapir has not developed yet, the entire salt overpressure dissipates along the source layer, leaving no salt overpressure at the diapir base at the left of the model. As the source layer loses its uniform thickness (Fig. 4c, d), the salt-overpressure dissipation also loses its uniform gradient (time = 35 Ma, 50 Ma; Fig. 7a). This gradient increases where the source layer is thinner, far from the diapir, and decreases in areas where the source layer is thicker, near the diapir; as a result, salt overpressure is high in thinner areas and low in thicker ones. As the source layer continues to thin non-uniformly (Fig. 4e), salt overpressure increases in thinner areas far from the diapir and decreases to almost zero in thicker areas near the diapir (time = 65 Ma; Fig. 7a). When the source layer becomes nearly welded (very thin) over an area (Fig. 4f), salt overpressure increases with a high gradient over this area and remains almost zero in thicker areas near the diapir (time = 80 Ma; Fig. 7a). After the source layer welds (Fig. 4g, h), salt overpressure remains negligible in most of the diapir pedestal (time = 85 Ma, 100 Ma; Fig. 7a). Even the salt overpressure near the weld tip becomes negligible as the weld tip propagates toward the diapir (Points T, T′; time = 85 Ma, 100 Ma; Fig. 7a). These results show that when the source layer thins and welds, salt pressure is disproportionately high in the thin areas of the source-layer and almost isostatic in the thick areas.

3.2.2. Salt pressure vs. overburden stress

Overburden stress, typically used to estimate stresses in geological structures (Zoback, 2010), depends on overburden thickness and density. However, in a welding source layer, salt overpressure and, thus, total salt pressure depend on source-layer thickness and geometry (Fig. 7a), implying that salt pressure in the source layer could differ from overburden stress. To investigate this implication, we compare salt pressure to overburden stress along the horizontal line passing through the middle of the source layer at different times during source-layer thinning and welding (Fig. 7b). Overburden stress at each point along the line is calculated from the thickness of salt and sediments overlying the point and the density profile used for them (Fig. 2).

Salt pressure in the source layer differs significantly from overburden stress as this layer thins and welds. At early stages, salt pressure changes almost linearly along the source layer (time = 20 Ma, 35 Ma; Fig. 7a). Overburden stress also changes almost linearly along the source layer (Fig. 4b, c). Because of similar variations, salt pressure and overburden stress become equal along the source layer (time = 20 Ma, 35 Ma; Fig. 7b). When the source layer thins (Fig. 4d–f), salt-pressure variation becomes nonlinear, increasing where the source layer is thin and decreasing where the source layer is thick (time = 50 Ma, 65 Ma, 80 Ma; Fig. 7a). This results in salt pressure that is higher than overburden stress in thin areas and lower than overburden stress in adjacent thick areas (time = 50 Ma, 65 Ma, 80 Ma; Fig. 7b). The ratio of salt pressure to overburden stress increases to nearly one near the diapir because salt pressure, due to overpressure vanishing, and overburden stress, due to basin vanishing, both equal the salt-overburden stress. When the source layer welds (Fig. 4g, h), salt pressure in the pedestal remains lower than overburden stress (time = 85 Ma, 100 Ma; Fig. 7b).

Lateral redistribution of basin weight allows for the imbalance between salt pressure and overburden stress. When salt in the source layer supports the weight of the overburden column above it, salt pressure equals overburden stress. Thus, where salt pressure is lower than overburden stress (basin columns near diapir; time = 65–100 Ma;

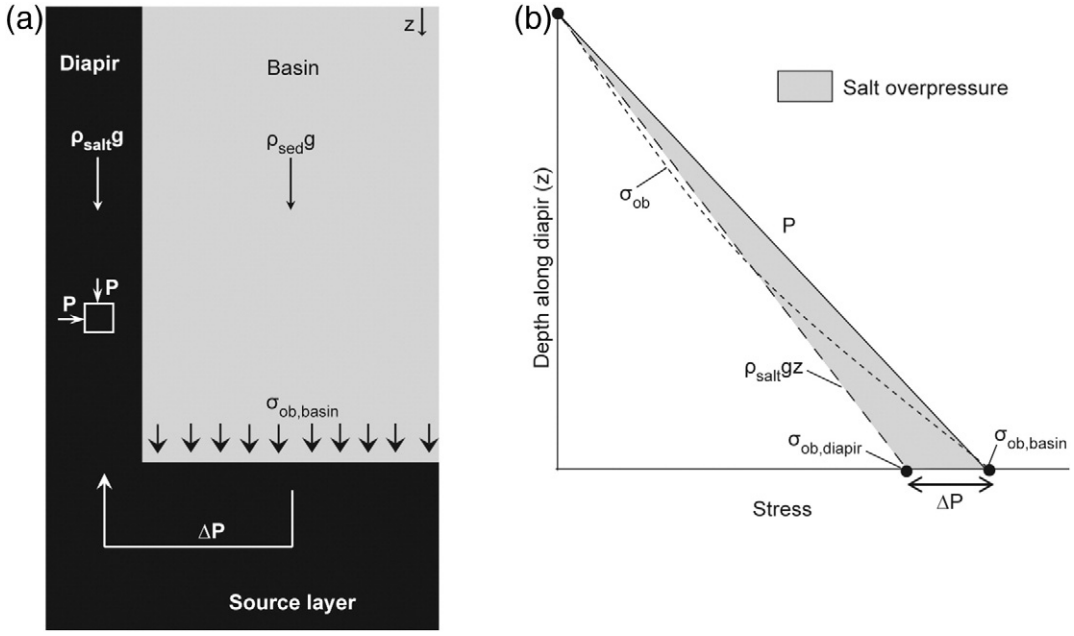

Fig. 5. A simplified model of a salt diapir with a thick source layer. (a) Model set-up. (b) Stresses along salt diapir and adjacent basin. In withdrawing source layers, source layer is overpressured relative to diapir. Salt flow transmits this overpressure into diapir, resulting in diapir salt pressure (P) greater than its overburden stress.

Fig. 7b), salt supports part of its overburden weight; where salt pressure is higher (basin columns far from diapir; time = 65–100 Ma; Fig. 7b), salt supports additional overburden weight. In fact, the weight of overburden is laterally redistributed from areas of low salt pressure to areas of high salt pressure (Fig. 7b). In other words, basin columns underlain by a thin salt layer support basin columns underlain by a thick salt layer. Basin shear strength allows for shear stress between basin columns, and these stresses laterally transfer the weight of basin overburden (Fig. 8). This redistribution is well established in engineering as *arching*, which is critical to transferring overburden above tunnels laterally through tunnel walls.

Overburden arching continues after source-layer welding. The basin over the weld supports the basin over the diapir pedestal, which prevents pedestal overburden from overpressuring salt in the pedestal (time = 85 Ma, 100 Ma; Fig. 7a). Salt does not evacuate the pedestal if not overpressured. Thus, overburden arching across the weld tip explains why pedestals persist around diapirs despite their substantial overburden (Hudec and Jackson, 2011).

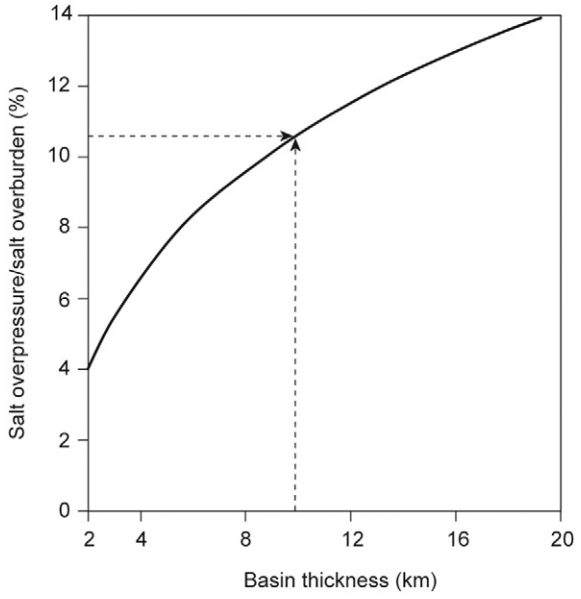

Fig. 6. Magnitude of salt overpressure, ΔP, relative to diapir overburden stress, calculated by using Eq. (1) and density profiles of salt and sediments (Fig. 2).

3.2.3. Horizontal stress in diapir-flank sediments

Because of stress continuity at the diapir-sediment interface, horizontal stress in sediments adjacent to the vertical flanks of the diapir is defined by salt pressure in the diapir (Fig. 9). Source-layer welding affects salt pressure in the diapir and thus horizontal stress in diapir-flank sediments. Before the source layer thins and welds, salt pressure in the diapir is greater than salt overburden stress because of the salt overpressure supplied by the source layer (time = 50 Ma and earlier; Fig. 7). After the source layer thins and welds, salt overpressure in the diapir almost vanishes (time = 65 Ma and later; Fig. 7a), decreasing salt pressure in the diapir and thus horizontal stress in sediments adjacent to diapir flanks.

Despite the decrease in diapir salt pressure after source-layer welding, horizontal stress in sediments adjacent to diapir flanks remains high. In sediments far from salt, where they are assumed under no lateral tectonic pressure, horizontal stress is a fraction of overburden stress (Fig. 10) (Zoback, 2010). In sediments near the salt diapir, horizontal stress, defined by diapir salt pressure, reduces to salt overburden stress after the diapir source layer thins and welds (Fig. 10). Despite this reduction, horizontal stress in diapir-flank sediments is still higher than horizontal stress in sediments far from the diapir (Fig. 10). Salt overburden stress is the minimum value of salt pressure in a diapir, meaning that horizontal stress in sediments adjacent to diapir flanks is always greater than horizontal stress in sediments far from the diapir.

4. Stress in near-weld sediments

Stresses are concentrated near the weld tip (Fig. 4g, h). In fact, vertical, horizontal, and shear stresses are all strongly perturbed (Fig. 11). The stress perturbation extends for a few kilometers across the weld tip and has a sharp gradient within a few hundred meters of the tip (Fig. 11).

The stress concentration relates to lateral redistribution of basin weight (arching) across the weld tip from basin over the pedestal to

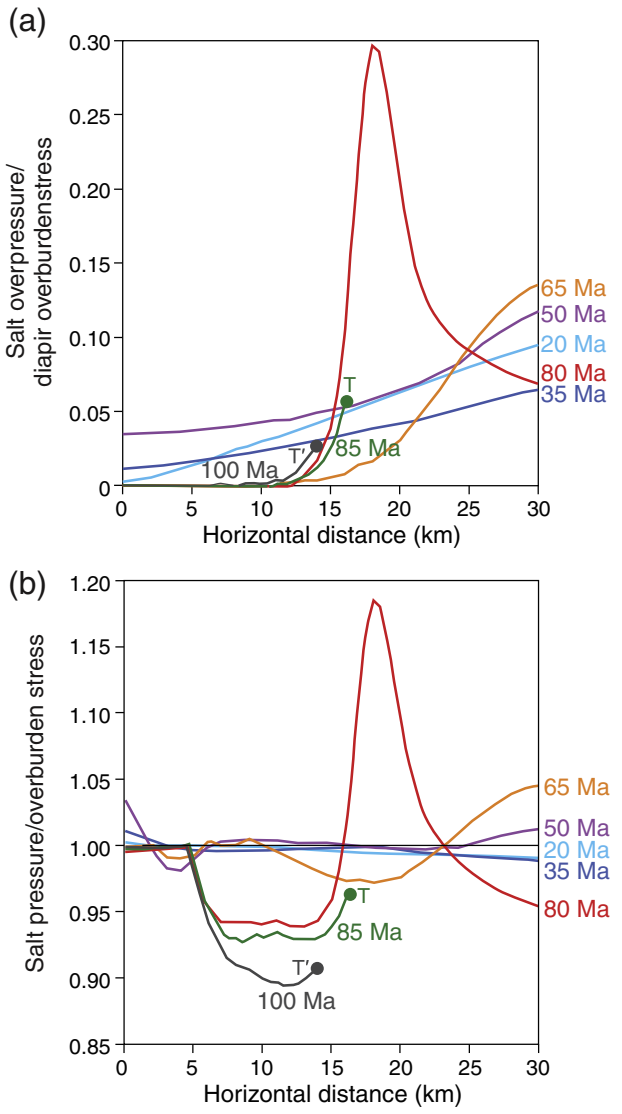

Fig. 7. Variation of salt pressure along middle of source layer in numerical model at different stages before and after source-layer welding. (a) Salt overpressure relative to diapir overburden at each stage. (b) Salt pressure relative to overburden stress from overlying salt and sediments.

basin over the weld. The redistribution reduces vertical stress over the pedestal and increases it over the weld (σ'_v; Fig. 11a). The increase is greatest at the weld tip and reduces away from the tip, over the weld. Arching also leads to anticlinal bending of unsupported basin over the pedestal, which causes compressional horizontal stress at the bottom of the basin and extensional horizontal stress at higher elevations

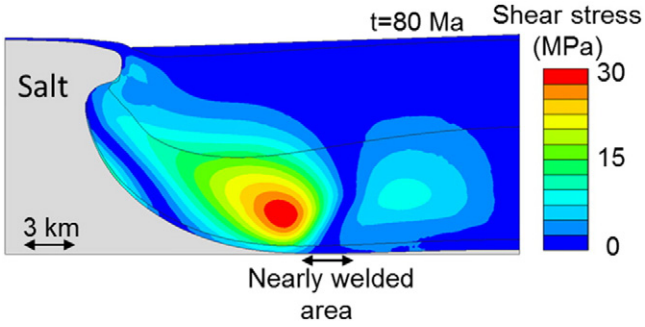

Fig. 8. Shear stress along vertical lines in basin. Contours indicate overburden arching from basin over pedestal and over nearly welded area.

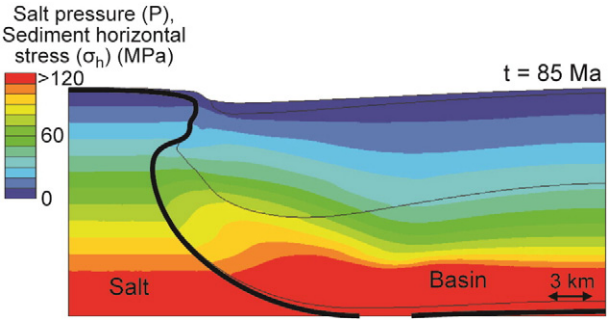

Fig. 9. Salt pressure in diapir vs. horizontal stress in adjacent sediments.

(along A-A′; Fig. 4h). Horizontal stress increases when approaching the weld tip along the base of the pedestal basin (σ'_h; Fig. 11a). Because horizontal and vertical stresses change differently across the weld tip, the ratio between them varies across the weld tip (Fig. 11b). The stress ratio is always higher than its regional value ($k_0 = 0.8$) because horizontal stress is perturbed everywhere more than vertical stress. Shear stress also increases over the pedestal toward the weld tip and decreases over the weld away from the tip (Fig. 11c). Because vertical stress decreases and horizontal stress increases over the pedestal, mean stress remains almost unchanged in that area (Fig. 11d). However, mean stress rises near the weld tip because of the increase in both vertical and horizontal stresses (Fig. 11d). The increase in mean stress and the shear stress causes compression of sediments and thus a decrease in their porosity (Fig. 11e).

Arching of basin overburden across the weld tip causes high shear stress above the tip (along dashed line C-C′; Fig. 12). Because sediments become stiffer and stronger with depth, shear stress increases with depth, reaching a maximum at the weld tip (Fig. 12b). High shear stress above the weld tip leads to a near-vertical zone of high shear deformation (Fig. 12a). This zone moves with the weld tip as welding continues toward the diapir.

All sediments over the weld experience weld-tip stress concentration when the tip propagates through them. The stress path at a

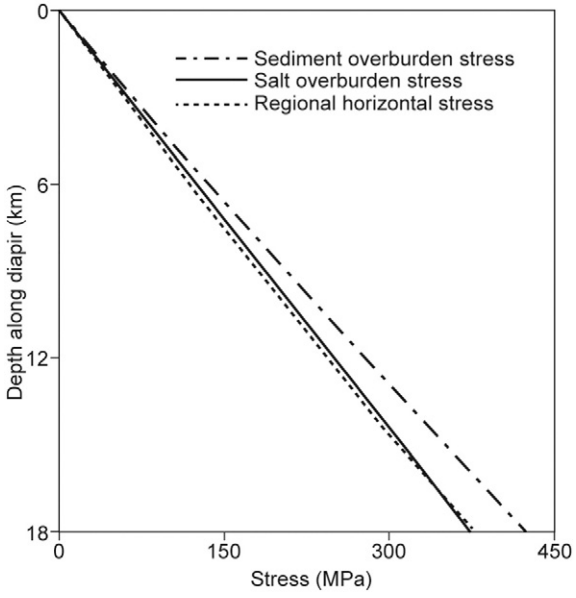

Fig. 10. Comparison of horizontal stress in sediments near and far from diapir, after diapir source layer thins and welds. In sediments near diapir, horizontal stress equals salt overburden stress. In sediments far from diapir, horizontal stress is a fraction of sediment overburden stress. This fraction is a function of ratio between effective horizontal and vertical stress (k_0). In our model, $k_0 = 0.8$.

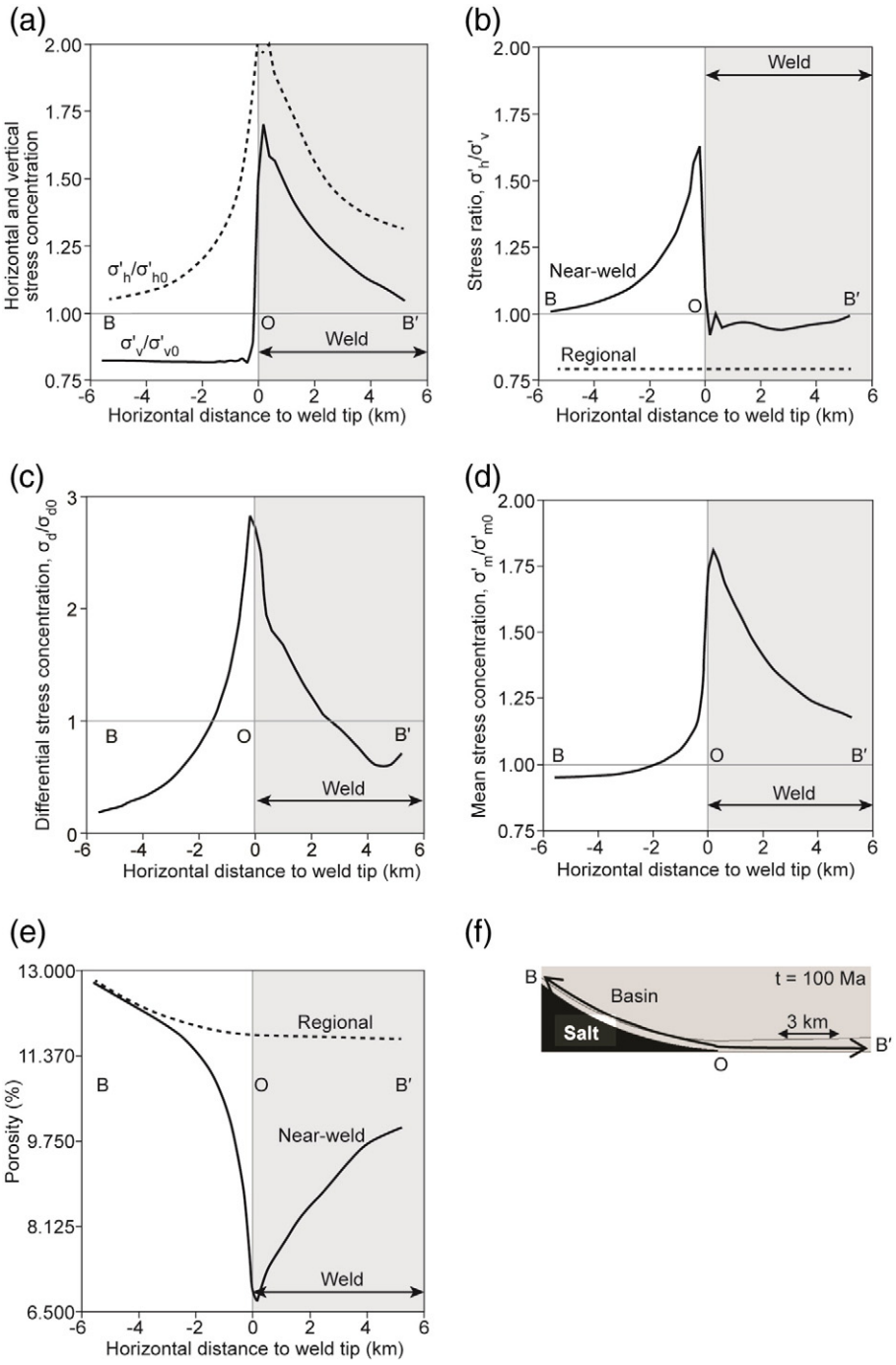

Fig. 11. Stress variation near weld tip at 100 Ma, along line B-B′ (sub–[e]), relative to regional values (designated with subscript $_0$). Regional values for a point on B-B′ are calculated assuming that sediments overlying point have been deposited with no lateral displacement (uniaxial deposition). (a) Horizontal (σ'_h) and vertical (σ'_v) stresses. (b) Ratio of horizontal to vertical stresses vs. regional value ($k_0 = 0.8$). (c) Shear stress. (d) Mean stress. (e) Porosity. (f) Cross section of studied area.

sediment point currently over the weld (Point W; Fig. 13a) illustrates this occurrence (Fig. 13b). Shear stress is lowest when the sediment point is over the pedestal (Point P; Fig. 13a, b), reaches a maximum when the weld tip is at the point (Point T; Fig. 13a, b), and then decreases to a residual value as the weld tip moves away and the point lies over the weld (Point W; Fig. 13a, b). During this time, mean stress continues to increase because of ongoing sedimentation.

5. Discussion

We simulate welding of a salt source layer and show its effects on adjacent sediments. As welding occurs, arching of basin overburden across the weld tip causes stress concentration at the tip (Figs. 11–13). This stress concentration results in material changes in sediments near the weld tip (Figs. 11e, 12a) and, consequently, in all sediments over the weld, considering that the weld tip propagates along the entire weld. A model that simulates only present weld geometry does not account for the temporal development of the weld and thus will fail to predict material changes in supraweld sediments.

Our prediction of local sediment compaction near welds (Fig. 11e) has been observed in wellbores drilled through or near source-layer welds (Hoetz et al., 2011). Sonic velocity data from 23 such wells in the Zechstein salt basin, northern Netherlands, showed increased velocities of up to 18% that could not be explained by factors other than the

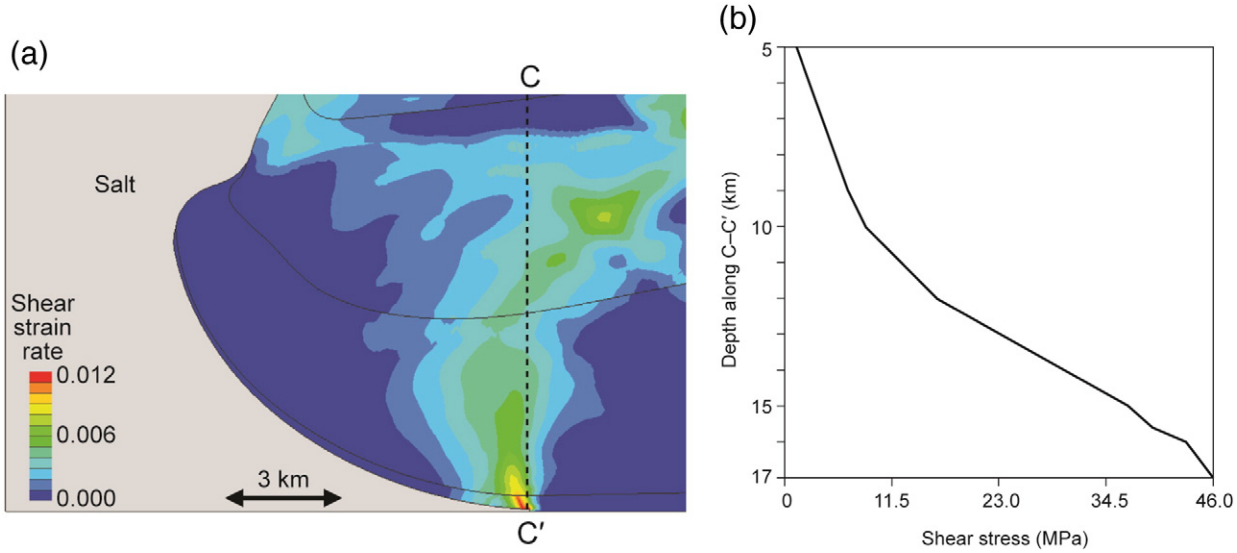

Fig. 12. Shearing above weld tip. (a) Contours of shear strain rate. (b) Shear stress along profile C-C′ in (a). Shear stresses induced by basin overburden arching across weld tip produce a potential for vertical faulting above tip.

welding. The increased velocities correspond to a reduction in porosity of 1–4%. Often, local increase in velocity of strata near welds is not considered in the velocity-depth models, which could result in erroneous pull-up of subweld strata (see Fig. 28 in Jones and Davison, 2014).

Our model predicts a near-vertical zone of high shear-strain rate above the weld tip (Fig. 12a), which suggests the potential for a fault emanating from the weld tip and propagating with a steep dip into higher sediments (Albertz and Sanz, 2012). We also show that this zone propagates with the weld tip as it moves along the weld toward the salt diapir. Faults are irreversible features, so they remain after the weld tip moves. Thus, our model illustrates that the supraweld basin might be populated with a parallel series of steeply dipping faults, upwardly decreasing in intensity (Fig. 12a). This prediction is consistent with the vertical faults observed over the welded zone of salt source layers around domes in the East Texas Basin (Maione, 2001). In agreement with our analysis, these faults were interpreted to result from the subsidence of the over-pedestal basin as salt withdraws from the pedestal (see Fig. 14 in Maione, 2001).

Such vertical faults may be used to help identify the geometry of salt welds and adjacent salt diapirs, where seismic data are usually uncertain. It is well known that the stem of a salt diapir is likely to be interpreted unrealistically as narrow or welded (teardrop shape) because of poor imaging near salt flanks (Jackson and Lewis, 2012; Jones and Davison, 2014). For instance, the salt domes with welded source layers in the East Texas Basin were interpreted to have such a teardrop shape (Maione, 2001), meaning that the weld around these domes extends all the way to their center (indicating a dome with almost no pedestal) (see Fig. 13 in Maione, 2001). However, vertical faults were found nearly 4 miles away from the center of the domes. According to our results, these faults develop over the weld, suggesting that the weld around these domes must start 4 miles away from the center of the domes, where the vertical faults begin. Consequently, these domes must have pedestals extending 4 miles from the center of the domes. This suggestion is additionally supported by our previous deduction that the complete removal of salt dome pedestals, as predicted by the seismic interpretation, is unlikely, particularly in tectonically neutral basins like the East Texas Basin.

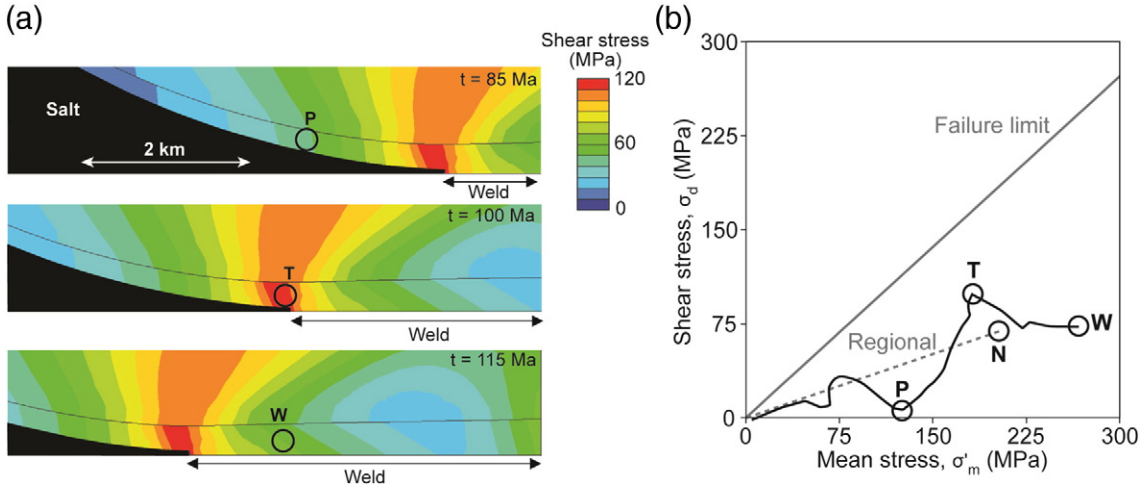

Fig. 13. Stress path at sediment point over weld. (a) Propagation of weld tip and associated stress concentration across sediment point near weld. Points P, T, and W show location of same sediment point at three different stages during weld propagation. Point is over pedestal at 85 Ma (P), at weld tip at 100 Ma (T), and over weld at 115 Ma (W). Contours show shear stress. (b) Stress path for sediment point. Regional stress path (dashed line) is calculated assuming deposition to same depth as point but under no lateral displacement conditions (uniaxial deposition).

Welding of a salt layer has substantial implications for the exploration of hydrocarbon reservoirs near welded salt layers. Salt bodies are most often assumed to be seals against the migration of hydrocarbons. This sealing is less certain for salt welds, where salt thins or completely disappears (McBride et al., 1998). The sealing of welds has been shown to depend on several factors, including the permeability of adjacent strata and the structural features near the welds (Rowan, 2004). Our study shows that the welding process has a significant control on these properties. Our results show that, as a result of increase in the mean and shear stress, porosity of sediments over the weld decreases (Fig. 11e). This decrease is associated with lowering the permeability of sediments, thus increasing the weld sealing capacity. The improvement in weld sealing capacity might, however, be offset by possible enhanced fracturing of sediments near the weld. Our model does not simulate fracturing of sediments; however, we show that, in sediments over the weld, the maximum shear stress (Point T; Fig. 13b) is higher than what is produced under regional conditions (Point N; Fig. 13b), and therefore weld sediments might have a higher degree of fracturing. Similar considerations of sediment compaction and fracturing may be used to evaluate the productivity of reservoirs near welds. The porosity and, thus, productivity of these reservoirs should be expected to decrease because of promoted compaction of the sediments and to increase because of possible promoted fracturing of the sediments (Hoetz et al., 2011). Possible vertical faults populated above welds is another implication of welding for exploration of hydrocarbon reservoirs near welds. These faults can act as vertical pathways for hydrocarbon migration and alter the prospectivity of structures around welds (Maione, 2001). The prospects created by these fault systems are often overlooked because they are located in the unattractive synclinal settings above welds and also because detection of such faults in seismic data is difficult (Maione, 2001). Finally, failure to consider the velocity increase of near-weld sediments in depth-velocity models is also a source of error in exploration of hydrocarbon reservoirs near welds. Such a failure led to underestimating the depth of a subweld reservoir in the Southern North Sea (Hoetz et al., 2011). The gas-bearing interval for a well drilled to this reservoir was too small, which made the well completion uneconomic.

To our knowledge, this is the first published example of an evolutionary model that simulates the development and propagation of a source-layer weld and studies the stress changes associated with this process. Further studies are needed to fully understand impacts of welding on salt systems under different conditions. For example, future models could take into account overpressure generation in sediments (Shumaker et al., 2014). Alternatively, the model could be extended to include pre-salt sediments and investigate not only subweld stress changes but also the effect of a nonrigid subweld section on welding. Sensitivity analyses with different material properties, deposition rates, and tectonic conditions will also extend our understanding of salt welds. Our model provides crucial insights into the mechanism of welding and its impact on the stresses and properties of adjacent sediments; such insights can improve interpretation of seismic and field data in salt systems with welded source layers.

6. Summary and conclusions

We use a forward evolutionary model to study stresses inside a salt diapir, its source layer, and their adjacent sediments as the source layer thins and welds. In the diapir, the salt isotropic stress state causes horizontal stress to equal overburden stress. Before welding, horizontal stress even exceeds salt overburden stress because of overpressure transmitted from the source layer. When the source layer thins and welds, dissipation along the layer leaves almost no salt overpressure for the diapir. Nonetheless, horizontal stress in the diapir and thus in diapir-flank sediments remains higher than the regional horizontal stress.

Dissipation along the source layer also changes the salt pressure in the layer. Because dissipation concentrates in the thin areas of the source layer, salt pressure in these areas becomes greater than overburden stress; in adjacent thick areas, salt pressure is less than overburden stress. To accommodate the resulting imbalance, basin strength allows for lateral redistribution of basin weight from areas with negative imbalance (over thick source layer) to those with positive imbalance (over thin source layer).

After welding, the weight of the pedestal basin is laterally transferred across the weld tip to the supraweld basin. This transfer causes a considerable stress concentration in sediments at the weld tip and consequently in all sediments along the weld, considering that the weld tip propagates through these sediments. This stress concentration and the resulting material changes affect the weld seal capacity, the stability of wellbores, the productivity of reservoirs, and the interpretation of seismic data near such welds.

Our results highlight that salt flow and basin strength are important to the prediction of stresses and behavior of salt systems, particularly those with a welding source layer. By taking into account these characteristics, we offer a better understanding of source-layer welding; its impacts on stresses; and its consequences for interpretation, exploration, and production near welded source layers.

Nomenclature

Symbol	Name	Dimension
ρ_{sed}	Sediment bulk density	L^{-3} M
ρ_{salt}	Salt density	L^{-3} M
g	Gravitational acceleration constant	LT^{-2}
z	Depth below basin surface	L
$\sigma_{ob,\ diapir}$	Diapir overburden stress	$L^{-1}MT^{-2}$
$\sigma_{ob,\ basin}$	Basin overburden stress	$L^{-1}MT^{-2}$
ΔP	Salt overpressure in thick source layer	$L^{-1}MT^{-2}$

Acknowledgments

The project was funded by the Applied Geodynamics Laboratory (AGL) consortium and The University of Texas at Austin (UT) GeoFluids consortium. AGL is supported by the following companies: Anadarko, Apache, BHP Billiton, BP, CGG, Chevron, Cobalt, Condor, ConocoPhillips, Ecopetrol, ENI, ExxonMobil, Fugro, Hess, ION, Lukoil, Maersk, Marathon, McMoRan, Murphy, Nexen, Noble, Pemex, Petrobras, PGS, Repsol-YPF, Samson, Saudi Aramco, Shell, Statoil, Talisman, TGS, Total, Venari, and Woodside. UT GeoFluids is supported by the following companies: Anadarko, BHP Billiton, BP, Chevron, ConocoPhillips, ExxonMobil, Hess, Murphy, Schlumberger, Shell, Statoil, and Total. This publication was authorized by the Director, Bureau of Economic Geology, Jackson School of Geosciences, The University of Texas at Austin.

Appendix A. Material parameters in the numerical model

Table A.1
Material parameters used for salt according to the Munson–Dawson model (Fredrich et al., 2007; Munson, 1997; Munson and Dawson, 1979).

Parameter	Unit	Value
E	MPa	10,000
ν	–	0.35
ρ	Kg/m^3	2100
A_1	1/Ma	1.885E36
n_1	–	5.5
Q_1	cal/mol	25,000
A_2	1/Ma	2.17E26
n_2	cal/mol	5.0
Q_2	–	10,000
R	cal/°C/mol	1.987

Table A.1 (*continued*)

Parameter	Unit	Value
T_0	°C	10
T_{const}	°C	273
G_0	MPa	12,400
dG/dT	GPa/°K	10.0

Table A.2
Material parameters used for sediments according to the SR3 model (Nygard et al., 2006; Nygard et al., 2004; Rockfield, 2010).

Parameter	Unit	Value
E	MPa	40
ν	–	0.25
K_0	MPa	10
κ	–	0.01
$p_{t,0}$	MPa	0.085
$p_{c,0}$	MPa	−1.00
β	Degrees	60.00
ψ	Degrees	51.00
β_0	–	0.60
β_1	1/MPa	0.725
α	–	0.25
N	–	1.3
n_0	–	0.38
Hardening properties		Fig. A.1

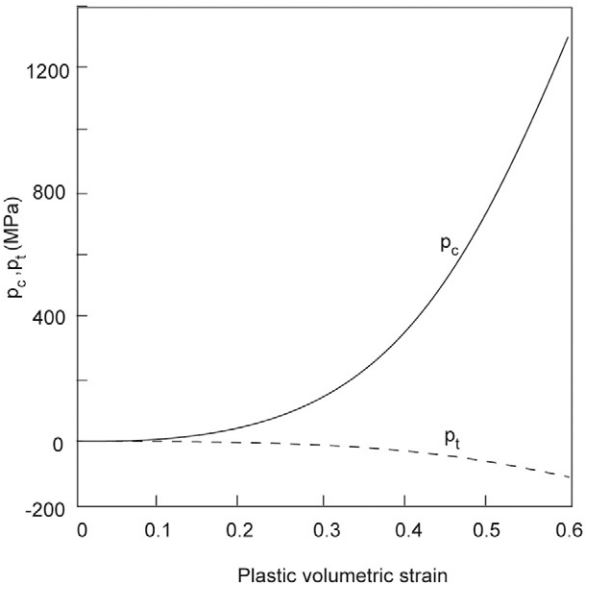

Fig. A.1. Input hardening properties in the SR3 model (Rockfield, 2010).

Table A.3
Unit conversion.

Metric system	Conversion	English system
m	/0.3048	Ft
kg	/0.4536	Lb
N	/4.448	Lbf
kPa	/6.895	Psi
Pa	/47.88	Psf
kN/m^3	/0.1572	Pcf

References

Albertz, M., Sanz, P.F., 2012. Critical state finite element models of contractional fault-related folding: part 2. Mechanical analysis. Tectonophysics 576–577, 150–170.

Boggs, S., 2010. Principles of Sedimentology and Stratigraphy. fifth ed. Prentice Hall, Upper Saddle River, NJ.

Crook, A.J.L., Willson, S.M., Yu, J.G., Owen, D.R.J., 2006. Predictive modelling of structure evolution in sandbox experiments. J. Struct. Geol. 28, 729–744.

Dusseault, M.B., Maury, V., Sanfilippo, F., Santarelli, F.J., 2004. Drilling Around Salt: Risks, Stresses, and Uncertainties, U.S. Rock Mechanics and Geomechanics Symposium. American Rock Mechanics Association, Houston, TX.

Fredrich, J.T., Fossum, A.F., Hickman, R.J., 2007. Mineralogy of deepwater Gulf of Mexico salt formations and implications for constitutive behavior. J. Pet. Sci. Eng. 57, 354–374.

Gray, G.G., Morgan, J.K., Sanz, P.F., 2014. Overview of continuum and particle dynamics methods for mechanical modeling of contractional geologic structures. J. Struct. Geol. 59, 19–36.

Heidari, M., Nikolinakou, M.A., Flemings, P.B., Hudec, M.R., 2015. A Simplified Analysis of Stresses in Rising Salt Domes and Adjacent Sediments, 49th U.S. Rock Mechanics and Geomechanics Symposium, San Francisco.

Heidari, M., Nikolinakou, M.A., Flemings, P.B., Hudec, M.R., 2016. A simplified stress analysis of rising salt domes. Basin Res., pp. 1–14.

Hoetz, G., Steenbrink, J., Bekkers, N., Vogelaar, A., Luthi, S., 2011. Salt-induced stress anomalies: an explanation for variations in seismic velocity and reservoir quality. Pet. Geosci. 17, 385–396.

Hudec, M.R., Jackson, M.P.A., 2011. The Salt Mine: A Digital Atlas of Salt Tectonics: The University of Texas at Austin, Bureau of Economic Geology. Udden Book Series No. 5.

Huffman, A.R., Bowers, G.L., Geologists, A.A.P., Engineers, A.A.D., 2002. Pressure regimes in sedimentary basins and their prediction. AAPG Mem. 76.

Jackson, C.A.-L., Lewis, M.M., 2012. Origin of an anhydrite sheath encircling a salt diapir and implications for the seismic imaging of steep-sided salt structures, Egersund Basin, northern North Sea. J. Geol. Soc. 169, 593–599.

Jackson, C.A.-L., Rodriguez, C.R., Rotevatn, A., Bell, R.E., 2014. Geological and geophysical expression of a primary salt weld: an example from the Santos Basin, Brazil. Interpretation 2, SM77–SM89.

Jackson, P.A., Talbot, C.J., 1991. A Glossary of Salt Tectonics. The University of Texas at Austin, Bureau of Economic Geology.

Jones, I.F., Davison, I., 2014. Seismic imaging in and around salt bodies. Interpretation 2, SL1–SL20.

Langlois, W.E., Deville, M.O., 2014. Slow Viscous Flow. second ed. Springer International Publishing, Cham, Switzerland.

Luo, G., Nikolinakou, M.A., Flemings, P.B., Hudec, M.R., 2012. Near-salt stress and wellbore stability: a finite-element study and its application, 46th U.S. Rock Mechanics and Geomechanics Symposium. American Rock Mechanics Association, Chicago, IL.

Maione, S.J., 2001. Discovery of ring faults associated with salt withdrawal basins, Early Cretaceous age, in the East Texas Basin. Lead. Edge 20, 818–829.

McBride, B.C., Weimer, P., Rowan, M.G., 1998. The effect of allochthonous salt on the petroleum systems of northern Green Canyon and Ewing Bank (offshore Louisiana), northern Gulf of Mexico. AAPG Bull. 82, 1083–1112.

Muir Wood, D., 1990. Soil Behaviour and Critical State Soil Mechanics. Cambridge University Press, Cambridge, U.K.

Munson, D.E., 1997. Constitutive model of creep in rock salt applied to underground room closure. Int. J. Rock Mech. Min. Sci. 34, 233–247.

Munson, D.E., Dawson, P.R., 1979. Constitutive Model for the Low Temperature Creep of Salt (With Application to WIPP), SAND79-1853. Sandia National Laboratories, Albuquerque, NM.

Nikolinakou, M.A., Flemings, P.B., Hudec, M.R., 2014. Modeling stress evolution around a rising salt diapir. Mar. Pet. Geol. 51, 230–238.

Nygard, R., Gutierrez, M., Bratli, R.K., Hoeg, K., 2006. Brittle-ductile transition, shear failure and leakage in shales and mudrocks. Mar. Pet. Geol. 23, 201–212.

Nygard, R., Gutierrez, M., Gautam, R., Hoeg, K., 2004. Compaction behavior of argillaceous sediments as function of diagenesis. Mar. Pet. Geol. 21, 349–362.

Peel, F.J., 2014. How do salt withdrawal minibasins form? Insights from forward modelling, and implications for hydrocarbon migration. Tectonophysics 630, 222–235.

Peric, D., Crook, A.J.L., 2004. Computational strategies for predictive geology with reference to salt tectonics. Comput. Methods Appl. Mech. Eng. 193, 5195–5222.

Perić, D., Vaz Jr., M., Owen, D.R.J., 1999. On adaptive strategies for large deformations of elasto-plastic solids at finite strains: computational issues and industrial applications. Comput. Methods Appl. Mech. Eng. 176, 279–312.

Rockfield, 2010. ELFEN Forward Modeling User Manual. Rockfield Software Limited.

Rowan, M.G., 2004. Do salt welds seal? Salt Sediment Interactions and Hydrocarbon Prospectivity: Concepts, Applications, and Case Studies for the 21st century: 24th Annual. Society of Economic Paleontologists and Mineralogists, pp. 390–403

Rowan, M.G., Lawton, T.F., Giles, K.A., 2012. Anatomy of an exposed vertical salt weld and flanking strata, La Popa Basin, Mexico. Geol. Soc. Lond., Spec. Publ. 363, 33–57.

Shumaker, N., Haymond, D., Martin, J., 2014. Kinematic linkage between minibasin welds and extreme overpressure in the deepwater Gulf of Mexico. Interpretation 2, SB69–SB77.

Thornton, D.A., Crook, A.J.L., 2014. Predictive modeling of the evolution of fault structure: 3-D modeling and coupled geomechanical/flow simulation. Rock Mech. Rock. Eng. 47, 1533–1549.

Thornton, D.A., Roberts, D.T., Crook, A.J.L., Yu, J.G., 2011. Regional Scale Salt Tectonics Modelling: Bench-Scale Validation and Extension to Field-Scale Problems., Beyond balanced sections: Geological Society of America Conference, Minneapolis, USA.

Wagner, B.H., 2010. An Analysis of Salt Welding. The University of Texas at Austin, Jackson School of Geosciences, p. 218.

Zoback, M.D., 2010. Reservoir Geomechanics. Cambridge University Press.